LETTER

ECOLOGY LETTERS · cnrs · WILEY

Reading tea leaves worldwide: Decoupled drivers of initial litter decomposition mass-loss rate and stabilization

Judith M. Sarneel[1,2] | Mariet M. Hefting[2] | Taru Sandén[3] | Johan van den Hoogen[4] | Devin Routh[4,5] | Bhupendra S. Adhikari[6] | Juha M. Alatalo[7] | Alla Aleksanyan[8] | Inge H. J. Althuizen[9,10] | Mohammed H. S. A. Alsafran[7] | Jeff W. Atkins[11] | Laurent Augusto[12] | Mika Aurela[13] | Aleksej V. Azarov[14] | Isabel C. Barrio[15] | Claus Beier[16] | María D. Bejarano[17] | Sue E. Benham[18] | Björn Berg[19] | Nadezhda V. Bezler[20] | Katrín Björnsdóttir[21] | Martin A. Bolinder[22] | Michele Carbognani[23] | Roberto Cazzolla Gatti[24,25] | Stefano Chelli[26] | Maxim V. Chistotin[27] | Casper T. Christiansen[28,29] | Pascal Courtois[30] | Thomas W. Crowther[4] | Michele S. Dechoum[31] | Ika Djukic[32] | Sarah Duddigan[33] | Louise M. Egerton-Warburton[34] | Nicolas Fanin[12] | Maria Fantappiè[35] | Silvano Fares[36] | Geraldo W. Fernandes[37,38] | Nina V. Filippova[39] | Andreas Fliessbach[40] | David Fuentes | Roberto Godoy[41] | Thomas Grünwald[42] | Gema Guzmán[43,44] | Joseph E. Hawes[45,46,47] | Yue He[48,49] | Jean-Marc Hero[50,51] | Laura L. Hess[46] | Katja Hogendoorn[52] | Toke T. Høye[53] | Wilma W. P. Jans[54] | Ingibjörg S. Jónsdóttir[55] | Sabina Keller[56] | Sebastian Kepfer-Rojas[16] | Natalya N. Kuz'menko[57] | Klaus S. Larsen[16] | Hjalmar Laudon[58] | Jonas J. Lembrechts[59] | Junhui Li[60,61] | Jean-Marc Limousin[62] | Sergey M. Lukin[63] | Renato Marques[64] | César Marín[65] | Marshall D. McDaniel[66] | Qi Meek[67] | Genrietta E. Merzlaya[27] | Anders Michelsen[28,68] | Leonardo Montagnani[69,70] | Peter Mueller[71,72] | Rajasekaran Murugan[73,74] | Isla H. Myers-Smith[75,76] | Stefanie Nolte[77,78] | Raúl Ochoa-Hueso[79] | Bernard N. Okafor[80] | Vladimir V. Okorkov[63] | Vladimir G. Onipchenko[81] | María C. Orozco[82] | Tina Parkhurst[83] | Carlos A. Peres[77] | Matteo Petit Bon[84,85,86] | Alessandro Petraglia[23] | Martin Pingel[87] | Corinna Rebmann[88] | Brett R. Scheffers[89] | Inger Schmidt[16] | Mary C. Scholes[90] | Efrat Sheffer[91] | Lyudmila K. Shevtsova[27] | Stuart W. Smith[92,93] | Adriano Sofo[94] | Pablo R. Stevenson[95] | Barbora Strouhalová[96] | Anders Sundsdal[92,97] | Rafael B. Sühs[98] | Gebretsadik Tamene[99] | Haydn J. D. Thomas[77] | Duygu Tolunay[2] | Marcello Tomaselli[23] | Simon Tresch[100] | Dominique L. Tucker[101,102] | Michael D. Ulyshen[103] | Alejandro Valdecantos[104,105] | Vigdis Vandvik[9] | Elena I. Vanguelova[106] | Kris Verheyen[107] | Xuhui Wang[48] | Laura Yahdjian[108,109] | Xaris S. Yumashev[110] | Joost A. Keuskamp[2,111]

For affiliations refer to page 11.

Correspondence
Judith M. Sarneel, Department of Ecology
and Environmental Science, Umeå
University, Umeå, Sweden.
Email: judith.sarneel@umu.se

Abstract
The breakdown of plant material fuels soil functioning and biodiversity. Currently, process understanding of global decomposition patterns and the drivers of such patterns are hampered by the lack of coherent large-scale datasets. We buried 36,000 individual litterbags (tea bags) worldwide and found an overall negative correlation between initial mass-loss rates and stabilization factors of plant-derived carbon, using the Tea Bag Index (TBI). The stabilization factor quantifies the degree to which easy-to-degrade components accumulate during early-stage decomposition (e.g. by environmental limitations). However, agriculture and an interaction between moisture and temperature led to a decoupling between initial mass-loss rates and stabilization, notably in colder locations. Using TBI improved mass-loss estimates of natural litter compared to models that ignored stabilization. Ignoring the transformation of dead plant material to more recalcitrant substances during early-stage decomposition, and the environmental control of this transformation, could overestimate carbon losses during early decomposition in carbon cycle models.

KEYWORDS
citizen science, environmental drivers, global change, litter decomposition, mass loss, soil organic matter formation, stabilization, tea bag index

INTRODUCTION

Large amounts of leaf litter are continuously deposited on soils, where it is broken down by biological and physical processes, releasing carbon dioxide and nutrients. Litter breakdown or decomposition is thus important for plant growth, soil functioning and biodiversity (Bardgett & van der Putten, 2014), while also playing a key role in global carbon and nutrient cycling (Stockmann et al., 2015). However, not all material in litter is decomposed (Li et al., 2023). What remains in the soil contributes to soil organic matter formation, and the magnitude of this contribution under prevailing and future climate conditions is heavily debated (Cotrufo et al., 2015; Minasny et al., 2017).

Plant litter is often classified as easy-to-degrade or recalcitrant. However, any litter material consists of a certain fraction of easy-to-degrade components (e.g. sugar and polysaccharides) as well as a certain fraction of more recalcitrant substances (e.g. lignin or acid-unhydrolysable material). After an initial fast mass loss in which the decomposition of easy-to-degrade material dominates, the accumulation of microbial necromass and secondary metabolites slows down the decomposition process (Berg & McClaugherty, 2020; Cotrufo et al., 2013). In some systems, recalcitrant compounds are generally considered to decompose completely, but over much longer time frames than easy-to-degrade material, ultimately driving long-term carbon cycling (Cotrufo et al., 2013). In several global carbon cycle models, different litter compounds are thus modelled with specific decomposition rates, which are usually estimated from low-resolution datasets with limited geographical cover (Le Noë et al., 2023; Sanchez et al., 2009). This creates uncertainties in model outcomes and large, uniform datasets are crucial to

impart hitherto poorly understood interactions between environmental factors, litter quality and decomposition (Heimann & Reichstein, 2008; Le Noë et al., 2023). These limitations in our current understanding of litter decomposition are reflected in the large range (50%–71%) of variation in mass loss explained by either litter type, climate or their combination across existing global studies (Berg et al., 1993; Djukic et al., 2018; Kwon et al., 2021; Parton et al., 2007; Trofymow et al., 2002).

In an alternative approach, Keuskamp et al. (2013) assume that each fresh litter is a mixture of material components. Initial mass losses are predominantly driven by loss of the easy-to-degrade components whereas mass loss due to decomposition of recalcitrant material fractions primarily drive long-term decomposition rates. Further, they conceptualize breakdown of the easy-to-degrade material by an initial mass-loss rate ($k1_{TBI}$; following terminology used in carbon cycle models for early-stage decomposition) and a stabilization factor (S_{TBI}). The stabilization factor quantifies the degree to which easy-to-degrade litter components accumulate and become more resistant, either because the given environmental conditions hamper their decomposition or because they are created during initial decomposition (e.g. as rest-products or necromass). The stabilization factor is, therefore, equivalent to a limit factor or stable residue (Berg & McClaugherty, 2020; Li et al., 2023). While the stabilization factor cannot directly be equated with long-term carbon storage as it describes initial litter breakdown dynamics, soils with a high stabilization factor should have a higher likelihood to accumulate a larger proportion of the easy-to-degrade litter components compared to soils with a low stabilization factor. Both $k1_{TBI}$ and S_{TBI} should, therefore, be considered integrative, location-specific estimators of soil functioning

that incorporate effects of leaching and microbial activity. In addition, both parameters describe the decomposition of easy-to-degrade litter compounds rather than the decomposition of a species-specific plant material, which allows for generalization and comparative analyses. Keuskamp et al. (2013) further proposed that $k1_{TBI}$ and S_{TBI} can be determined empirically using standardized litter (tea), in a method referred to as the Tea Bag Index (TBI; Box 1) which further facilitates standardized, large-scale comparative studies. The TBI thus has great potential as a generalizable approach to understand initial mass-loss dynamics across biomes and/or environmental gradients, which in turn, can improve predictions of soil carbon dynamics in present and future environmental settings.

The collective efforts of citizen scientists and the scientific community brought together over 36,000 tea bag decomposition measurements across almost 2000 1 km^2 pixels distributed across all major terrestrial biomes worldwide (Figure 1). This database enables us to provide the largest empirical analysis of initial mass-loss dynamics worldwide. We hypothesise that if microbial activity is a key underlying driver of both $k1_{TBI}$ and S_{TBI}, those proxies will be correlated and respond to environmental factors in a similar way. This would imply that environmental conditions that increase $k1_{TBI}$ will decrease S_{TBI} and vice versa. Alternatively, if microbial activity affects $k1_{TBI}$ and S_{TBI} through different mechanisms, or if other processes (e.g. leaching) play a more important role for early mass loss of plant residues, $k1_{TBI}$ and S_{TBI} could be decoupled. Next, in order to explore the possibilities for upscaling (e.g. for carbon modelling), we spatially interpolated our measured TBI proxies using random forest models into two predictive maps. From this, we calculated the amount of leaf-derived carbon potentially subjected to stabilization globally. Lastly, we evaluated if the stabilization factor can be used to estimate mass losses of other (local) litter types.

MATERIALS AND METHODS

Tea Bag Index method

The TBI defines the easy-to-degrade material as the hydrolysable fraction obtained from a fractionation analysis (Keuskamp et al., 2013). This fraction decomposes with an initial mass-loss rate ($k1_{TBI}$) towards a stabilization factor (S_{TBI}), describing the fraction of hydrolysable compounds that, due to the conditions at that location, is judged to be more recalcitrant to decomposition (Box 1). This distinguishes the TBI model from a single-phase model where all litter fractions are assumed to decompose completely (Gholz et al., 2000; Le Noë et al., 2023), as well as from an ordinary two-phase model, where all easy-to-degrade material is assumed to be decomposed relatively quickly (Li et al., 2023). The TBI method uses the mass loss of a rapidly decomposing standardized leaf litter, green tea, to calculate S_{TBI} after 3 months incubation (Box 1). The mass loss of a more slowly decomposing leaf litter, rooibos tea, is used to obtain $k1_{TBI}$, as for most environments, 3 months is not sufficient for this litter type to decompose as far as S_{TBI} (obtained from green tea) allows.

Following the standardized TBI protocol (Keuskamp et al., 2013), at least one bag of Lipton® green tea (EAN: 87 22700 05552 5) and at least one bag of Lipton® rooibos tea (EAN: 87 22700 18843 8) with woven nylon mesh (0.257 mm) were buried at 8 cm depth and around 15 cm apart at each location. The bags were retrieved after ca. 90 days (median 90 days; the 10%–90% percentile was 56–101 days) and cleaned from adhering soil particles without using water. Roots were removed and the remaining dry mass (30–70°C for >48 h) of the tea inside the bags was determined. Starting masses obtained by participants were confounded by local ambient air moisture as bags could not be dried before the start. We, therefore, used a standard starting dry mass for green (1.732 ± 0.062 s.d. g) and rooibos (1.865 ± 0.047 s.d. g), which was based on the moisture content determined by drying (60°C for >48 h) additional, new, not-incubated tea bags from different batches and countries ($n = 708$ pairs of tea bags).

Handling of global data

Mass-loss data for over 36,000 individual tea bags was collected using strict TBI protocols across the participating network to ensure data quality (Table S1). We defined an incubation as unique combinations of GPS location (WGS84), duration (days), start date and user-defined location name. While incubations typically deployed 3–12 replicates, we used mean incubation mass loss to calculate the Tea Bag Index (TBI) following Keuskamp et al. (2013; Box 1) as this decreased random variation associated with very local differences and/or measurement error. We further included data from 27 studies reporting mass losses, $k1_{TBI}$ and S_{TBI}, or that were willing to share such data associated with a specific GPS location (Table S2).

We excluded and did not collect incubations with (i) explicit and small-scale experimental treatments applied (e.g. warming, plant removal; excluding 29 unique GPS locations), (ii) incubation duration <45 or >135 days (excluding 88 unique GPS locations). Moreover, we excluded incubations (iii) with invalid TBI proxies (negative $k1_{TBI}$ values or S_{TBI} values larger than one; excluding 51 unique GPS locations). See Figures S1 and S2 for climatic and spatial distribution of excluded locations. Incubations from soils under agricultural use (169 unique GPS locations; Figure S3) were included since (i) these incubations represent globally common soil types and (ii) many types of land management (e.g. forestry, grazing, mowing) may frequently not be reported explicitly. Incubations that

BOX 1   Calculations of the Tea Bag Index.

The Tea Bag Index (TBI) assumes that initial mass-loss rates of litter are driven by the decay of easy-to-decompose, early-stage material and decrease towards $1 - a$, where a represents the stable residue or recalcitrant fraction of the material, typically represented by the lignified, acid insoluble fraction of the material (Li et al., 2023; Parton et al., 2007). However, in the TBI this term represents the acid insoluble fraction *plus* the fraction of the remaining (potentially hydrolysable) material that has become more recalcitrant to further breakdown (e.g. due to environmental limitations to decomposition, as rest-products of breakdown or as necromass).

The remaining mass proportion $M(t)$ of the litter after t days follows:

$$M(t) = a e^{-kt} + (1 - a) \tag{1}$$

where k is the mass-loss rate of the fraction that will eventually break down. Since mass-loss rates of green tea slow down considerably after 1–2 months (Keuskamp et al., 2013), it can be used to calculate the fraction that will break down (a_g):

$$a_g = 1 - \frac{M_g(t)}{M_g(0)} \tag{2}$$

where $M_g(0)$ is the starting weight of green tea. The fraction of the potentially degradable material that is stabilized (S_{TBI}) is subsequently calculated by scaling the mass loss to the hydrolysable fraction of green tea (0.842; H_g) obtained from Keuskamp et al. (2013):

$$S_{TBI} = 1 - \frac{a_g}{H_g} = 1 - \frac{M_g(0) - M_g(t)}{H_g * M_g(0)} \tag{3}$$

Subsequently, S_{TBI} is applied on the hydrolysable fraction of rooibos tea (0.552; H_r), allowing calculation of the potential degradable fraction of rooibos tea (a_r) as:

$$a_r = H_r \left(1 - S_{TBI} \right) \tag{4}$$

Finally, a_r and the remaining mass fraction of rooibos tea are used to derive $k1_{TBI}$ from Equation 1. Our $k1_{TBI}$ thereby represents the initial mass-loss dynamics of the potentially degradable material. By using S_{TBI}, it takes into account that the environmental conditions do not allow breakdown of a part of the hydrolysable fraction on this timescale. Over longer timescales the stabilized but potentially degradable material may or may not be broken down, and mass losses from the recalcitrant fraction may occur.

The TBI method relies on two basic assumptions (Keuskamp et al., 2013). Firstly, the incubation duration is assumed to be short enough for rooibos to still be decomposing hydrolysable material, and long enough for green tea to decompose all the hydrolysable material that can be decomposed. In practice, this proves to be 45–135 days. From decomposition curves in tundra systems we know that 30–45 days is sufficient for green tea to reach a plateau (Thomas et al., 2023; Figure S14) while incubations of 1 year or longer lead to enhanced decomposition in green tea. Second, the TBI method assumes the transfer of S_{TBI} across litter types. Chemical extractions using nuclear magnetic resonance spectroscopy confirm that remains of the hydrolysable compounds (e.g. carbohydrates and cellulose) accumulate over time in an order of magnitude that can explain stabilization (Duddigan, Shaw, et al., 2020). Lignin-like substances on the other hand, barely decompose during the standard TBI incubation period of 90 days (Duddigan, Shaw, et al., 2020). We explore the transfer of S_{TBI} across litter types further in the main text.

were located in the terrestrial part of coastal zones were included, but aquatic incubations were excluded.

We aggregated the $k1_{TBI}$ and S_{TBI} of incubations that fell within the same 30 arcsec pixels (approximately 1 km^2 at the equator; Figure S4). This resulted in mean $k1_{TBI}$ and S_{TBI} in, respectively, 1643 and 1716 unique pixels across the globe (Figure 1) with a good spatial, temporal and climatic coverage (Figure 1b,c; Tables S3 and S4).
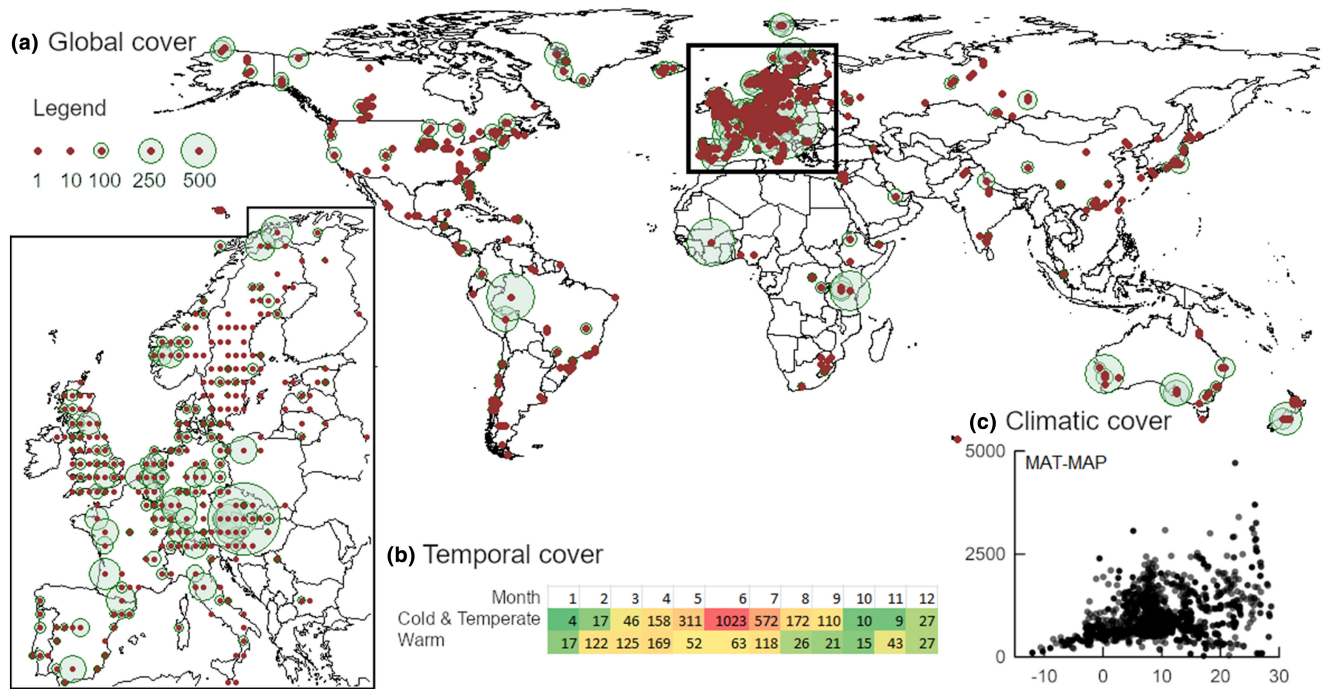
FIGURE 1 Sampling distribution of the global Tea Bag Index experiment across (a) space, (b) time and (c) climate. In total 65 countries were sampled including measurements from all biomes. Each brown dot represents one location, with the green circle indicating the number of valid measurements at that location. In the insert for Europe, sample locations are gridded to increase readability. The colour scale in subfigure B indicates the number of locations from a few (green) to many (red) summed per month of the year for cold and temperate biomes [see Figure 2 for biome classification which follows Olson et al. (2001)] and for warm (including dry and tropical) biomes. Measurements from the northern and southern hemisphere have been aligned by the winter solstice so that the first month is January for incubations in the northern hemisphere and July for the southern hemisphere. Each black dot represents mean annual air temperature (MAT) and mean annual precipitation (MAP) for locations with measurements as obtained from the WorldClim database.

Global covariate layers

Given the large number of contributors and citizen participation, map-based data were used to provide consistent estimates of environmental conditions to avoid observer bias or missing values. We extracted 125 ecologically relevant global products (covariate layers) from different sources (see Table S5) and unified them to a 30 arcsec pixel grid (roughly 1 km^2) in EPSG:4326 (WGS84). These layers included global patterns in climate (e.g. mean annual air and soil temperature, mean annual precipitation), vegetation productivity and abundance (e.g. net primary production, forest cover), anthropogenic landscape heterogeneity (e.g. population density, percentage developed land), topography (e.g. elevation, slope), spectral reflectance bands, topsoil chemistry (e.g. pH, cation exchange capacity) and topsoil physical parameters (e.g. bulk density). In addition, biomes were obtained from Olson et al. (2001).

Analysis of global patterns

To understand global patterns of $k1_{TBI}$ and S_{TBI} as well as their relationships with each other and with major environmental drivers, we tested for differences in means across biomes, between agricultural and non-agricultural soils,

and for relationships of the TBI proxies with mean annual soil temperature and precipitation, using Generalized Least Squares models (GLS). We focused on temperature and precipitation as they confound the major gradients in our environmental products (Figure S5) and are straightforward to interpret (Prescott, 2010). For all models, an exponential spatial autocorrelation structure was included after testing the best fit based on AIC-criteria (comparing: no, exponential, ratio, linear, gaussian or spherical spatial autocorrelation structures). Variograms show that this improved model performance in all tests (Figure S6). We transformed $k1_{TBI}$ using the natural logarithm in all analyses to meet model assumptions. A Tukey post hoc test was used to test differences between biomes (restricted to those where we had data from ≥10 unique pixels) and weighted biome means were calculated using 'emmeans' (Lenth et al., 2023).

Second, we ran a GLS model testing the relationship between $k1_{TBI}$ and S_{TBI} (including spatial autocorrelation following the procedure outlined above) and correlated the residuals to mean annual soil temperature and precipitation to evaluate what caused decoupling of $k1_{TBI}$ and S_{TBI}. For this latter we also used GLS, but we did not include a spatial autocorrelation structure as this was already accounted for by the model from which the residuals were derived. Last, we re-ran all models using mean annual air temperature.

Geospatial modelling

To explore spatial patterns of early mass-loss dynamics of plant litter and derive global maps of predicted TBI proxies, separate random forest models were built for S_{TBI} and ln-transformed $k1_{TBI}$, following the procedure outlined in van den Hoogen et al. (2019). We performed a grid search procedure to tune the random forest models across a range of 30 hyperparameter settings (with 2–10 variables per split and 2–6 as a minimum leaf population). For each of the 30 models, we assessed the model performance using k-fold cross-validation (using $k=10$; folds assigned randomly, stratified per biome to ensure equal representation of each bioclimatic zone). The mean coefficient of determination R^2 across the tested models was the basis for choosing the best model (van den Hoogen et al., 2019). The final image was subsequently calculated as a mean of the top 10 best performing hyperparameter settings. To generate coefficients of variation images (standard deviation divided by mean) that provide a per-pixel accuracy of our predicted TBI, we followed a stratified bootstrapping procedure (stratified per biome). After classifying the composite raster data 100 times, we used these to create per-pixel mean and standard deviation images. The resulting maps of predicted TBI proxies and associated models should be used to address large rather than small spatial scales.

To quantify the potential extrapolation of our TBI maps we assessed if the pixels with measurements covered the environmental conditions of the pixels without measurements, taking into account combinations of two environmental variables. To this end, we first performed a PCA using the 125 covariate layers for all pixels for which we had measurements (van den Hoogen et al., 2019). Second, we transformed all terrestrial pixels without measurements into the same PCA space by using scaling and centring the eigenvectors and values of the PCA. Third, we represented the sampled environmental conditions (interpolation) by creating PCA convex hulls enclosing the pixels with measurements. We did this for all bivariate combinations of the first 28 PCA axes (explaining >90% of the PCA-variation and resulting in 378 combinations). Last, for each pixel without measurements, we quantified a per-pixel degree of interpolation as the % of the convex hulls that included this pixel. Geospatial analyses and extrapolation were performed in Google Earth Engine and Python (Gorelick et al., 2017).

Global estimates

To assess the global magnitude of carbon in easy-to-degrade litter components that is subjected to stabilization per year, we first obtained six global maps of litter production (He et al., 2021). These include a measurement-based interpolation map in addition to equivalents to litter production from five well-accepted land surface models (CABLE, ISAM, JULES, OCN and ORCHIDEE) at a resolution of 1800 arcsec (0.5°). To account for the variation of litter quality, we took the median (0.72), upper quartile (0.80) and lower quartile (0.61) hydrolysable fraction from 145 plant species (Own measurements; Harmon, 2016; Robbins et al., 2022, see Figure S7). This proved a robust representation of the variation in litter quality and spanned the same range as the (unequally represented) growth forms (Figure S7). We then multiplied each pixel in each of the six global maps of litter production with the three hydrolysable fractions. Subsequently, we multiplied those 18 estimates with the predicted pixel S_{TBI} (unified to a 0.5-degree resolution). Last, we multiplied each pixel with the landmass of that pixel and summed values worldwide to obtain 18 estimates of global Gt C year^{-1} subjected to stabilization.

Using TBI to estimate local litter mass loss

We explored the hypothesis that the stabilization factor can be used to estimate mass losses from the hydrolysable fraction of any type of plant litter at a given location by making a comparison between measured local litter mass loss and predicted mass loss using the TBI proxies. To this end, we buried teabags and local leaf litter (four replicates of three litter types and two retrieval dates for local litter = 16 bags per location) at ten forests in a gradient from northern Finland to Italy in the European Integrated Carbon Observation System (ICOS) infrastructure (Figure S8; Table S6). Leaf litter from the dominant tree species at these locations (e.g. pine, oak, beech) was fragmented to <0.5 cm^2 and 2 g was, per species, enclosed in nylon mesh bags exactly identical to tea bags. Bags were buried between 26 April and 22 June 2016 following the TBI protocol (Keuskamp et al., 2013). Rooibos, green tea and local litter bags were retrieved after 90 days, and one more set of local litter bags after two growing seasons (380–457 days). This longer period was needed for local litter to reach stabilization because local litter resembled rooibos in composition, and rooibos also needed more than 90 days. The remaining litter dry mass was determined (60–70°C for 48 h), and $k1_{TBI}$ and S_{TBI} were calculated using the tea bags (Box 1).

We determined the hydrolysable fraction (g g^{-1}) by acid fractionation of four replicate samples of 1 g ground material of each litter type (ranging from 0.496 ± 0.026 S.E.M. to 0.708 ± 0.034 S.E.M.) as in Keuskamp et al. (2013). Subsequently, we predicted the decomposable fraction (a_L) and proportion of initial mass remaining at time t $M_L(t)$ for local litter at all locations for the days (t) that the local litter was incubated, using the locally measured $k1_{TBI}$ and S_{TBI} and the hydrolysable fraction of the local litters (H_L).

$$M_L(t) = a_L e^{-k1_{TBI}t} + (1 - a_L) \qquad (5)$$

With:

$$a_L = H_L\left(1 - S_{TBI}\right) \qquad (6)$$

We subtracted the calculated $M_L(t)$ from the observed remaining local litter mass. In this way, negative values indicate how much the TBI proxies overestimate the local litter mass loss. We contrasted the location means ($n = 10$) of the TBI-based estimates with a model without stabilization factor, assuming $a_L = H_L$. This assumes that eventually all hydrolysable material is broken down.

$$M_L(t) = H_L e^{-k1_L t} + \left(1 - H_L\right) \qquad (7)$$

Where $k1_L$ is the initial mass-loss rate determined using local litter mass loss after 90 days and its hydrolysable fraction. The estimations were tested with a paired t-test with location as pairing factor. All analyses were performed in R 4.3.1 (R Core Team, 2023).

RESULTS

Global drivers of initial mass-loss rate and stabilization factor

Across the global gradients covered by our dataset, we found that initial mass-loss rates increased as stabilization factors decreased, forming a strong negative correlation between $k1_{TBI}$ and S_{TBI}, (correlation coefficient $\ln(k1_{TBI})$ and $S_{TBI} = -0.97$; $p < 0.001$, Figure 2). This correlation reflected a shift from high initial mass-loss rates and a low
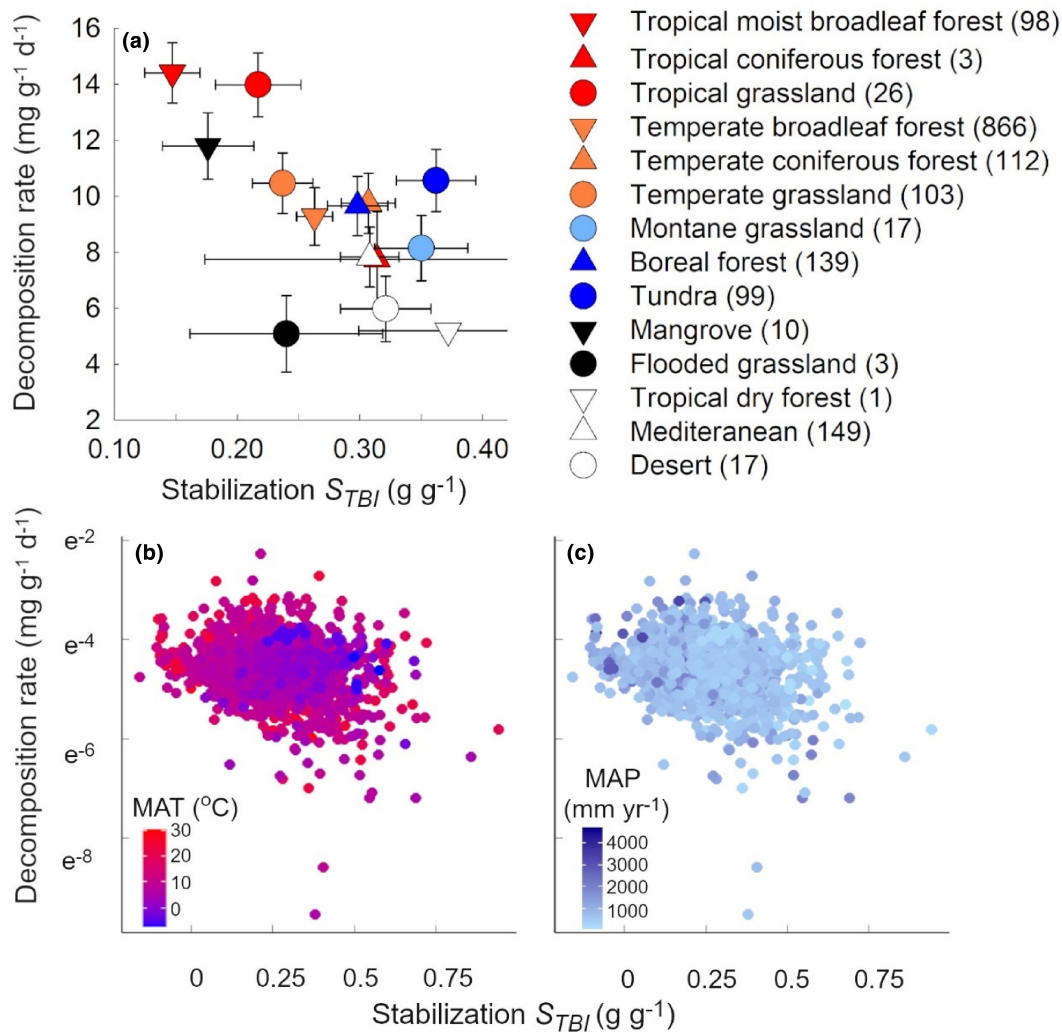
FIGURE 2 Deviations from the overall negative correlation between $k1_{TBI}$ and S_{TBI} of biomes and interactive effects of soil MAT and MAP. (a) Mean $k1_{TBI}$ and S_{TBI} per biome. Colour coding follows main climatic conditions, with red for tropical, orange for temperate, blue for cold, black for wetlands and white for dry ecosystems. Forest biomes are indicated by triangles and low vegetation system by circles. Values shown are corrected for spatial autocorrelation. Error bars are standard errors. Biome names follow Olson et al. (2001) with some abbreviations. Full biome names can be found in Table S4 and Tukey post hoc tests in Table S7. Numbers behind category names indicate the number of pixels per biome. (b) Scatter plot of $k1_{TBI}$ and S_{TBI} coloured by the mean annual soil temperature and (c) mean annual precipitation of the location. Hence, deviations of the overall correlation between $k1_{TBI}$ and S_{TBI} are determined by the interaction between soil MAT and MAP (F-ratio $= 13.35$, $p < 0.001$). See Table S8 for remaining statistics and the relations of the residuals with mean annual air temperature.

stabilization factor in warm tropic biomes (wet broadleaf forests, savannas) to low initial mass-loss rates and high stabilization factors in cold and dry biomes such as boreal forest and deserts (Figure 2a; Table S7).

Despite this strong general trend across climatic zones, rates and relationships varied across biomes. For example, the tundra biome had intermediate $k1_{TBI}$ values not differing significantly from any other biome (Table S7). However, its S_{TBI} was high; more than twice that of tropical moist broadleaf forest ($p < 0.001$) and mangroves ($p = 0.007$) and nearly twice that of temperate grasslands ($p = 0.060$) and tropical grasslands ($p = 0.074$; Table S7). Similarly, tropical grasslands and deserts had contrasting initial mass-loss rates ($p < 0.001$), but similar stabilization factors ($p = 0.57$).

Another deviation from the global trend across climatic zones was that mediterranean forests, boreal and temperate coniferous forests had very similar $k1_{TBI}$ and S_{TBI} values despite their very different climate conditions (Figure 2). Agricultural cultivation significantly increased $k1_{TBI}$ by 30% (GLS; $F_{1,1631} = 6,32$; $p = 0.012$), whereas S_{TBI} was not significantly affected (GLS; $F_{1,1704} = 2.282$; $p = 0.131$; Figure S9). Analysing the residuals of the relationship between $k1_{TBI}$ and S_{TBI} showed that deviations depend on climate (Figure 2b,c; Table S8). The modelled relationship underpredicts the observed $k1_{TBI}$ in cold and moist conditions, whereas $k1_{TBI}$ is overpredicted in warm and wet conditions (Table S8).

We found that both $k1_{TBI}$ and S_{TBI} were affected by the significant interaction between mean annual soil temperature and precipitation, but in different ways. Whereas $k1_{TBI}$ increased with both soil temperature and precipitation for globally relevant values, S_{TBI} decreased with both for soil temperatures larger than $-2.87°C$ but increased with precipitation for lower soil temperatures (Figure 3; Figures S10 and S11; Table S9). This implies that in cold locations, both $k1_{TBI}$ and S_{TBI} increase with increasing precipitation, whereas in warmer locations $k1_{TBI}$ increases and S_{TBI} decreases with increasing precipitation. Similar relationships were observed with mean annual air temperature (Figure S10).

Global patterns

Interpolation of the nearly 2000 pixels resulted in different spatial patterns (Figure 4) for $k1_{TBI}$ and S_{TBI}. While $k1_{TBI}$ was relatively high in the wet tropics, intermediate and relatively constant across the Arctic, boreal and temperate zones, and lowest in dry regions at intermediate latitudes, S_{TBI} was lowest in the wet tropics and generally increased towards colder and drier biomes. Important predictors for variation in $k1_{TBI}$ were soil temperature ranges, soil moisture, and mean annual soil temperature, whereas the most important predictor for S_{TBI} variation was the mean annual air temperature (Table S10). Overall, the 10-fold cross-validated R^2 was 0.29 ± 0.01 s.d. for $k1_{TBI}$
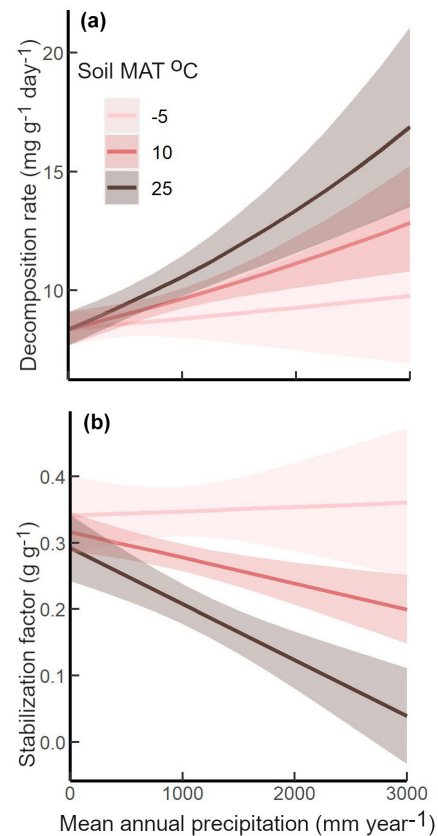
FIGURE 3 The interaction of both $k1_{TBI}$ and S_{TBI} with MAT and MAP causes decoupling in dryer and colder environments. Relationship between mean annual precipitation (MAP) and $k1_{TBI}$ (a) S_{TBI} (b) for different values of mean annual soil temperature (MAT), based on the models described in Table S9. Lines indicate the mean and the shaded areas the confidence intervals obtained using 'predictSE.gls' in the AICcmodavg package in R. Using mean annual air temperature resulted in similar patterns (Table S9; Figure S9).

and $R^2 = 0.61 \pm 0.03$ s.d. for S_{TBI}. Moreover, sampled pixels represented the global environmental conditions well and extrapolation was limited since 73% of the world's pixels fell within more than 95% of the PCA convex hull spaces that enclosed the sampled pixels. Outliers, that is falling within less than 25% of the PCA convex hulls, were mostly located in arid and polar regions (Figure S12).

We estimated that litter equivalent of 7.9–12.3 Gt carbon year^{-1} is subjected to stabilization globally (Figure S13) based on the six available global litter production estimates of He et al. (2021) and using a median hydrolysable fraction. Accounting for variation of the hydrolysable fraction increases the range to 6.7–13.7 Gt carbon year^{-1}. The measurement-based litter production map estimated from 7.2 to 9.4 Gt carbon year^{-1} (Figure S13).

Estimates of local litter decomposition

We found that using TBI proxies significantly improved estimations of mass loss compared to the ordinary two-phased model in which all the hydrolysable material will
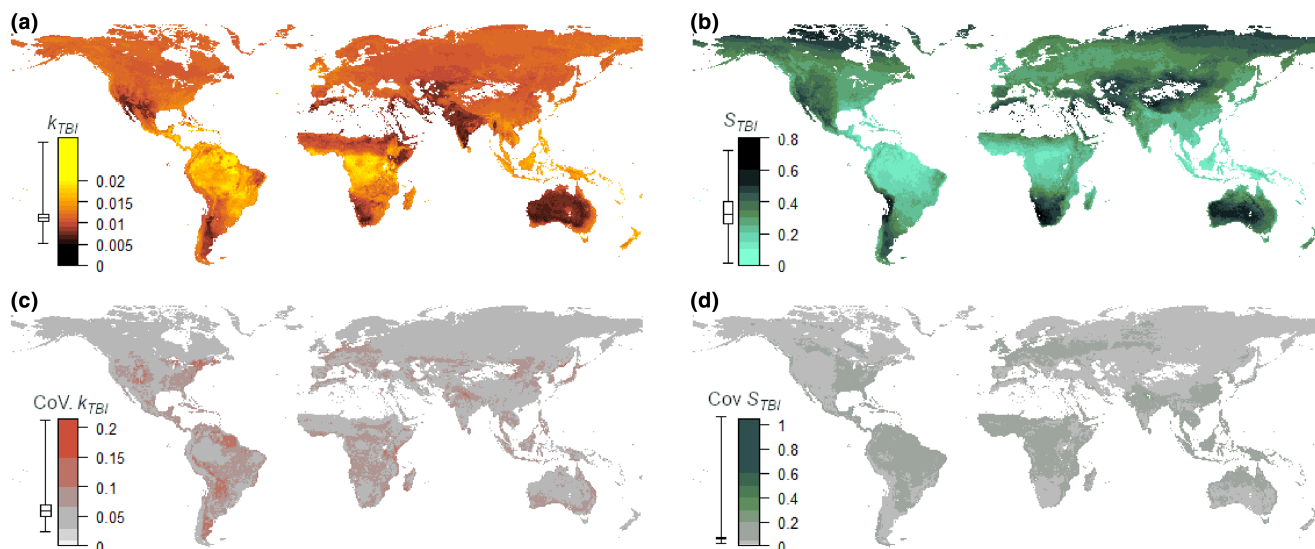
FIGURE 4 Global patterns of $k1_{TBI}$ and S_{TBI} differ and have a high accuracy. (a) Initial mass-loss rate ($k1_{TBI}$) and (b) the stabilization factor (S_{TBI}) of hydrolysable litter fractions and (c, d) accuracy of the predictions quantified as coefficient of variation (bootstrapped standard deviation divided by the mean predicted value). In panels (a) and (b), colours indicate predicted values with darker colours indicating lower initial mass-loss rates or higher stabilization factors. In panels (c) and (d), colours indicate the upper quartile of the bootstrapped coefficients of variation and thus lower accuracy of the prediction. Boxplots next to the scale indicate the quartile ranges and median of the mapped values. White areas were removed from the map due to extrapolation risks (Figure S11). Predictions of $k1_{TBI}$ had lowest accuracy in dry areas, whereas the accuracy of predictions of S_{TBI} was lowest around the equator.

eventually decompose (*t*-test; $t = -9.10$, d.f. $= 9$, $p < 0.001$). The ordinary two-phased model consistently overestimated mass loss in all locations (mean absolute difference in mass loss 20.9% ±1.9 SE). Using the TBI proxies reduced overestimation of mass losses (mean absolute difference in mass loss 8.6% ±2.6 SE), and differences ranged from a nearly exact match in a French and an Italian broadleaf forest to a 25.2% overestimation in a Dutch coniferous forest (Figure 5).

DISCUSSION

We found an overall negative correlation between initial mass-loss rate of hydrolysable fractions ($k1_{TBI}$) and the stabilization factor (S_{TBI}). Our large, standardized dataset further showed that $k1_{TBI}$ and S_{TBI} can vary independently of each other in specific climatic and environmental settings, implying a decoupling. The TBI proxies provided better estimates of mass loss of local litter compared to models that ignored stabilization, and on a global scale the amount of carbon subjected to stabilization is considerable.

Decoupling of initial mass-loss rate and stabilization

The two TBI proxies are strongly negatively correlated at a global scale. Hence, warm and moist conditions that typically enhance microbial activity (Prescott, 2010), resulted in both faster decomposition (higher initial rates) as well as a less material being left (lower stabilization
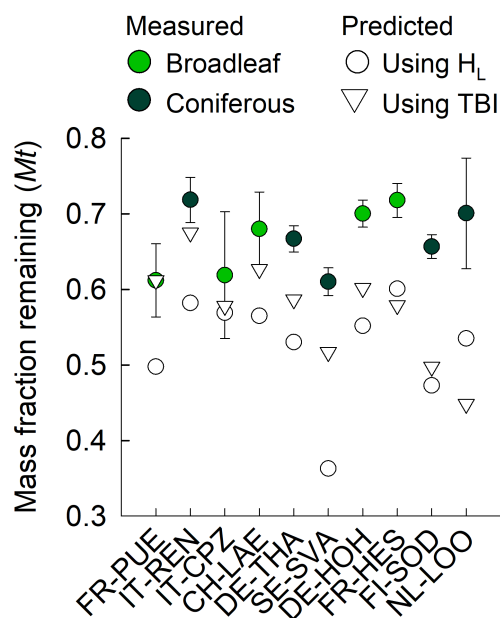

FIGURE 5 Addition of the stabilization factor improves mass loss predictions of local litter compared to models ignoring stabilization after two growing seasons in ICOS-forest locations (see Table S6 and Figure S8 for location details). Error bars are standard deviations of local litter measurements. Whereas an ordinary two-phase model (white circles) overpredicts mass losses of local litter in all locations, estimates using the TBI proxies (triangles) provide reasonable estimates of the local litter of about seven of the locations.

factor). However, we also observed that specific combinations of environmental factors (moisture gradients in cold environments) determine how much of the hydrolysable

fraction will disappear, while other factors (e.g. agriculture) determine the rate by which it is lost. These worldwide gradients match earlier descriptions of decoupled TBI proxies at local scales in boreal floodplains (Sarneel & Veen, 2017), wetlands (Mueller et al., 2018), grazed grasslands (Tang et al., 2020) and in fertilized soils (Ochoa-Hueso et al., 2020), and add new knowledge about intermediate mass-loss rates yet very high stabilization in the tundra biome compared to other biomes. Although poorly understood, differential effects of environmental conditions on decomposition have been reported for leaf litter as well. For instance, Hobbie et al. (2012) found that nutrient addition affected the degree to which oak leaves were decomposed (stabilization) more than the initial mass-loss rate of those leaves. Hence, our process-based approach and uniform global dataset puts what was previously suggested in regional or small-scale studies into a coherent global context and framework.

Although we lack direct evidence for a mechanism, we found indications for three potential mechanisms. First, specific conditions, (e.g. nutrient availability) could enhance degree of decomposition of the hydrolysable fraction (stabilization) or microbial nutrient use efficiency, while other conditions that co-vary with the first condition (water limitation, temperatures, oxygen deprivation) may inhibit initial mass-loss rates (Ochoa-Hueso et al., 2020; Sarneel & Veen, 2017). Second, decoupling could potentially occur when leaching provides a relative more important contribution to mass loss than microbial decomposition. For instance, due to cold conditions the tundra may have decreased microbial activity and hence relatively small mass losses (high stabilization factor). However, since leaching is a fast process (Gessner et al., 1999) that occurs without microbial activity, this may explain why we observed a relatively high initial mass-loss rate in the tundra. The water-soluble fraction of the tea used in TBI lies within the range observed in other tree species (Sarneel et al., 2023) and separating microbial decomposition from leaching, which is an inherent challenge in litter bag studies, is an emerging field (van den Brink et al., 2023). Third, our results suggest that a decoupling could result from non-climate factors associated with the vegetation (Althuizen et al., 2018), such as symbiosis with mycorrhizae, allelochemicals, priming, etc. (Bahram et al., 2020) based on absence of differences between coniferous biomes in different climate zones. Although further mechanistic studies are needed, the observed decoupling between initial rates and final degree of decomposition of easy-to-decompose litter components urges its implementation in carbon models. Opportunities to explore these critical aspects, with potential implications for ecosystem carbon cycling, are limited in current models.

In contrast to the ecological explanations provided above, Mori et al. (2022) argued that when the stabilization factor is not transferrable across litter types (an assumption underlying TBI; Box 1), this would lead to a decoupled, positive relationship between the TBI proxies. Since our TBI-based estimates of mass loss differed more than 10% from the observed in only three out of 10 forests, we assume that local, yet unknown, conditions may decrease the transferability of the stabilization factor. A global analysis on the size of the stable residue (which is equivalent to the stabilization factor; Li et al., 2023) suggest that initial leaf nitrogen and Mn concentrations were important for stable residue size, and presumably also for the stabilization factor. Since nutrients could facilitate mass loss of the hydrolysable fraction of the nutrient-poor rooibos more than that of green tea (Duddigan, Alexander, et al., 2020; Fanin et al., 2020; Kwon et al., 2021) they could indeed decrease the transferability of the stabilization factor. However, this is hard to quantify on a global scale and may have mostly affected $k1_{TBI}$ that depends on the transfer of the stabilization factor (e.g. a low R^2). We further know that a very long or short incubation time can restrict the transferability (Keuskamp et al., 2013), which we addressed by having rather narrow selection criteria for incubation duration.

Comparisons to local litter in our study suggest that local, yet unknown conditions may affect the transferability. For instance, home field advantages can arise from local interactions between litter quality and local decomposer communities (Veen et al., 2015), enhancing local litter decomposition. Yet, being non-local plant material to most systems, the TBI overcomes potential confounding effects that litter from more common plant species could have. So, although we do not exclude violations on a local scale, our observed strong negative relation between mass-loss rate and stabilization at a global level may indicate that the assumption on transferability holds. Hence the gained process understanding implies that decoupling should be considered when interpreting mass losses in natural litter, or assessing the decomposition responses to, for instance, changes in environmental conditions.

Initial mass-loss rates at a global scale

The effect of temperature and precipitation on initial mass-loss rate confirm the proposed hierarchal drivers (Prescott, 2010), where cold and dry climates have lower values and smaller variation in initial mass-loss rates. Roughly half of our measurements were from the (late) growing season (Figure 1). Hence, the pattern of relatively high initial mass-loss rates across temperate and polar zones may imply that the growing season in those regions generally provides favourable or even optimal conditions for decomposition. Yet, outside the growing season conditions may be less favourable or even stop decomposition (Thomas et al., 2023). Inferring from this, the increased growing season length associated with climate change (Post et al., 2019), may affect yearly decomposition rates in addition to other climate-related changes. Further considering the role of seasonality on early-stage litter breakdown is an important next step in our understanding of

what drives global patterns of hydrolysable litter mass loss and its feedback to carbon dioxide emissions and soil organic matter formation (Daebeler et al., 2022).

Stabilization at a global scale

While the stabilization factor does not directly predict soil organic matter dynamics, it can be seen as a first step towards incorporation of litter into soil organic matter. Our first global estimates of litter-derived carbon associated to stabilization yielded relevant and broadly realistic values. We are aware that those estimates need refinement through including photodegradation (Austin & Vivanco, 2006), fire and soil fauna (Njoroge et al., 2022), and biome-specific variation in litter quality. However, it is promising that the range of our study is strikingly similar to, for instance, the 'mean yearly accumulation of litter with resistance to decomposition' measured across 40 forests and grassland systems reviewed by Cebrian (1999) and in range with the 474 observations of stable residue size collected by Li et al. (2023). The common practice of overlooking the transformation of hydrolysable material to more recalcitrant fractions (Foley, 2005; Parton et al., 1998) or microbial necromass (Buckeridge et al., 2020) and in particular the differential effect of environmental drivers on initial mass-loss rates and the stabilization factor could lead to a potential bias in carbon cycle modelling. Our data, methods, and suggestions for future development needs are, therefore, important and relevant from a basic science and applied perspective.

CONCLUSIONS

Based on empirical litter decomposition data obtained at an unprecedented spatial scale, we demonstrate how the interaction between temperature and precipitation can decouple initial mass-loss rates and stabilization of litter-derived carbon. This bears important consequences under climate change, as this decoupling can result in context-dependencies in how warming affects ecosystem carbon cycling in colder environments, where environmental change is more extreme (IPCC, 2022). Further, we note that variation in empirical litter mass-loss data can result from a mixture of initial mass-loss rates, stabilization or even longer term dynamics (Joly et al., 2023). Hence, we believe that the TBI proxies and their underlaying global database provide powerful tools to aid process understanding as well as to train and improve global carbon models, especially regarding the role of climate context-dependencies and interactions.

AUTHOR CONTRIBUTIONS

AFFILIATIONS
[1]Department of Ecology and Environmental Science, Umeå Universitet, Umeå, Sweden
[2]Ecology and Biodiversity Group, Institute of Environmental Biology, Utrecht University, Utrecht, The Netherlands
[3]Department for Soil Health and Plant Nutrition, Austrian Agency for Health and Food Safety (AGES), Vienna, Austria
[4]Department of Environmental Systems Science, Institute of Integrative Biology, ETH Zürich, Zurich, Switzerland
[5]Science IT, University of Zürich, Zurich, Switzerland
[6]Department of Habitat Ecology, Wildlife Institute of India, Dehradun, India
[7]Environmental Science Center, Qatar University, Doha, Qatar
[8]Department of Geobotany and Plant Ecophysiology, Institute of Botany aft. A.L. Takhtajyan NAS of RA, Yerevan, Armenia
[9]Department of Biological Sciences and Bjerknes Centre for Climate Research, University of Bergen, Bergen, Norway
[10]NORCE Norwegian Research Centre AS, Bjerknes Centre for Climate Research, Bergen, Norway
[11]USDA Forest Service, Southern Research Station, New Ellenton, South Carolina, USA
[12]INRAE, Bordeaux Sciences Agro, ISPA, Villenave d'Ornon, France
[13]Finnish Meteorological Institute, Climate System Research, Helsinki, Finland
[14]Belgorod Federal Agrarain Scientific Center, Belgorod, Russia
[15]Faculty of Environmental and Forest Sciences, Agricultural University of Iceland, Reykjavík, Iceland
[16]Department of Geosciences and Natural Resource Management, University of Copenhagen, Copenhagen, Denmark
[17]Department of Natural Systems and Resources, Universidad Politécnica de Madrid, Madrid, Spain
[18]Forest Research, Surrey, UK
[19]Department of Forest Sciences, University of Helsinki, Helsinki, Finland
[20]All-Russian Institute of Sugar and Sygar Beet Named after D. Mazlumov, Ramon, Russia
[21]Department of Biological and Environmental Sciences, University of Gothenburg, Gothenburg, Sweden
[22]Department of Ecology, Swedish University of Agricultural Sciences (SLU), Uppsala, Sweden
[23]Department of Chemistry, Life Sciences and Environmental Sustainability, University of Parma, Parma, Italy
[24]Biological Institute, Tomsk State University, Tomsk, Russia
[25]Department of Biological, Geological and Environmental Sciences, University of Bologna, Bologna, Italy
[26]School of Biosciences and Veterinary Medicine, University of Camerino, Camerino, MC, Italy
[27]All-Russian Research Institute of Agrochemistry Named after D. Pryanishnikov, Moscow, Russia
[28]Center for Permafrost (CENPERM), Department of Geosciences and Natural Resource Management, University of Copenhagen, Copenhagen, Denmark
[29]Terrestrial Ecology Section, Department of Biology, University of Copenhagen, Copenhagen Ø, Denmark
[30]UMR Silva, INRAE, AgroParisTech, Université de Lorraine, Nancy, France
[31]Departamento de Ecologia e Zoologia, Universidade Federal de Santa Catarina, Florianópolis, SC, Brazil
[32]Swiss Federal Institute for Forest, Snow and Landscape Research WSL, Zurich, Switzerland
[33]Department of Geography and Environmental Science, University of Reading, Reading, UK
[34]Chicago Botanic Garden, Glencoe, Illinois, USA
[35]Consiglio per la Ricerca in Agricoltura e l'Analisi dell'Economia Agraria, Rome, Italy
[36]National Research Council of Italy Institute for Agriculture and Forestry Systems in the Mediterranean, Naples, Italy
[37]Departamento de Genética, Ecologia & Evolução, ICB/Universidade Federal de Minas Gerais, Belo Horizonte, MG, Brazil
[38]Knowledge Center for Biodiversity, Belo Horizonte, MG, Brazil
[39]Yugra State University, Khanty-Mansiysk, Russia
[40]Research Institute of Organic Agriculture, Frick, Switzerland

[41]Instituto de Ciencias Ambientales y Evolutivas, Universidad Austral de Chile, Valdivia, Chile
[42]Institute of Hydrology and Meteorology, TUD Dresden University of Technology, Tharandt, Germany
[43]Andalusian Institute of Agricultural and Fisheries Research and Training (IFAPA), Camino de Purchil, Granada, Spain
[44]Institute for Sustainable Agriculture-CSIC, Cordoba, Spain
[45]Applied Ecology Research Group, School of Life Sciences, Anglia Ruskin University, Cambridge, UK
[46]Earth Research Institute, University of California, Santa Barbara, California, USA
[47]Institute of Science and Environment, University of Cumbria, Ambleside, Cumbria, UK
[48]College of Urban and Environmental Sciences, Sino-French Institute for Earth System Science, Institute of Carbon Neutrality, Peking University, Beijing, China
[49]International Institute for Applied Systems Analysis (IIASA), Laxenburg, Austria
[50]School of Anthropology and Conservation, Durrell Institute of Conservation and Ecology, University of Kent, Canterbury, UK
[51]School of Science, Technology and Engineering, The University of the Sunshine Coast, Maroochydore, Queensland, Australia
[52]School of Agriculture, Food and Wine, The University of Adelaide, Adelaide, South Australia, Australia
[53]Department of Ecoscience and Arctic Research Centre, Aarhus University, Aarhus C, Denmark
[54]Wageningen Environmental Research, Wageningen, The Netherlands
[55]Institute of Life and Environmental Sciences, University of Iceland, Reykjavík, Iceland
[56]Department of Environmental Systems Science, ETH Zurich, Zurich, Switzerland
[57]Federal Scientific Center for Fiber Crops, Tver, Russia
[58]Department of Forest Ecology and Management, Swedish University of Agricultural Sciences, Umeå, Sweden
[59]Research Group Plants and Ecosystems (PLECO), University of Antwerp, Wilrijk, Belgium
[60]Center for Ecosystem Science and Society, Northern Arizona University, Flagstaff, Arizona, USA
[61]Department of Earth System Science, University of California, Irvine, California, USA
[62]CEFE, Univ Montpellier, CNRS, EPHE, IRD, Montpellier, France
[63]Upper Volga Federal Agrarain Scientific Center, Vladimir, Russia
[64]Departamento de Solos e Engenharia Agrícola, Universidade Federal do Paraná, Curitiba, Brasil
[65]Centro de Investigación e Innovación para el Cambio Climático (CiiCC), Universidad Santo Tomás, Valdivia, Chile
[66]Department of Agronomy, Iowa State University, Ames, Iowa, USA
[67]Department of Renewable Resources, Faculty of Agricultural, Life and Environmental Science, University of Alberta, Edmonton, Alberta, Canada
[68]Department of Biology, University of Copenhagen, Copenhagen Ø, Denmark
[69]Forest Services, Autonomous Province of Bozen-Bolzano, Bolzano, Italy
[70]Libera Universita di Bolzano, Facoltà di Scienze e Tecnologie, Piazza Università, Bolzano, Italy
[71]Smithsonian Environmental Research Center, Edgewater, Maryland, USA
[72]Institute of Plant Science and Microbiology, Universität Hamburg, Hamburg, Germany
[73]Soil Biology and Plant Nutrition, Faculty of Organic Agricultural Sciences, University of Kassel, Witzenhausen, Germany
[74]Valli Sustainability Research and Education, Kanchipuram, Tamil Nadu, India
[75]Department of Forest and Conservation Sciences, Faculty of Forestry, Forest Sciences Centre, University of British Columbia, Vancouver, British Columbia, Canada
[76]School of GeoSciences, University of Edinburgh, Edinburgh, Scotland, UK
[77]School of Environmental Sciences, University of East Anglia, Norwich, UK
[78]Centre for Environment, Fisheries and Aquaculture Science, Lowestoft, UK
[79]Department of Biology, IVAGRO, University of Cádiz, Campus de Excelencia Internacional Agroalimentario (ceiA3), Cádiz, Spain
[80]National Horticultural Research Institute, Ibadan, Nigeria
[81]Department of Ecology and Plant Geography, Biological Faculty, Lomonosov Moscow State University, Moscow, Russia
[82]Department of Biological Sciences, Universidad de los Andes, Bogotá, Colombia
[83]School of Environmental and Conservation Sciences, Murdoch University, Murdoch, Western Australia, Australia

[84]Department of Arctic Biology, The University Centre in Svalbard, Longyearbyen, Svalbard, Norway
[85]Department of Arctic and Marine Biology, Faculty of Biosciences Fisheries and Economics, The Arctic University of Norway, Tromsø, Norway
[86]Department of Wildland Resources, Quinney College of Natural Resources and Ecology Center, Utah State University, Logan, Utah, USA
[87]Department of Applied Ecology, Hochschule Geisenheim University, Geisenheim, Germany
[88]Helmholtz Centre for Environmental Research – UFZ, Leipzig, Germany
[89]Department of Wildlife Ecology and Conservation, University of Florida, Gainesville, Florida, USA
[90]School of Animal, Plant and Environmental Sciences, University of the Witwatersrand, Johannesburg, South Africa
[91]Institute of Plant Science and Genetics in Agriculture, The Hebrew University of Jerusalem, Rehovot, Israel
[92]Department of Biology, Norwegian University of Science and Technology, Trondheim, Norway
[93]Ecological Science Department, The James Hutton Institute, Aberdeen, UK
[94]Department of European and Mediterranean Cultures: Architecture, Environment, Cultural Heritage (DiCEM), University of Basilicata, Matera, Italy
[95]Universidad de Los Andes, Bogotá, Colombia
[96]Departement of Physical Geography and Geoecology, Faculty of Science, Charles University, Prague, Czech Republic
[97]Faculty of Technology, Natural Sciences and Maritime Sciences, University of South-Eastern, Notodden, Norway
[98]Programa de pós-graducão em Ecologia, Universidade Federal de Santa Catarina, Florianópolis, SC, Brazil
[99]Department of Natural Resource Management, College of Agriculture and Environmental, University of Gondar, Gondar, Ethiopia
[100]Institute for Applied Plant Biology, Witterswil, Switzerland
[101]Case Western Reserve University School of Medicine, Cleveland, Ohio, USA
[102]Center for Energy, Environment and Sustainability, Department of Biology, Wake Forest University, Winston-Salem, North Carolina, USA
[103]USDA Forest Service, Southern Research Station, Athens, Georgia, USA
[104]Department of Ecology, University of Alicante, Alicante, Spain
[105]Multidisciplinary Institute for Environmental Studies, Ramon Margalef, IMEM, University of Alicante, Alicante, Spain
[106]Centre for Forest Protection, Forest Research, Surrey, UK
[107]Department of Environment, Forest and Nature Lab, Gent University, Ghent, Belgium
[108]Cátedra de Ecología, Facultad de Agronomía, UBA, Buenos Aires, Argentina
[109]Instituto de Investigaciones Fisiológicas y Ecológicas Vinculadas a la Agricultura (IFEVA), Facultad de Agronomía, Universidad de Buenos Aires and CONICET, Buenos Aires, Argentina
[110]Chelyabinsk Agricultural Institute, Chelyabinsk, Russia
[111]Biont Research, Utrecht, The Netherlands

ACKNOWLEDGEMENTS

CONFLICT OF INTEREST STATEMENT

The authors have no conflict of interest to declare.

PEER REVIEW

The peer review history for this article is available at https://www.webofscience.com/api/gateway/wos/peer-review/10.1111/ele.14415.

DATA AVAILABILITY STATEMENT

The global summary data and the script to extract data from the standardized calculation sheets are published on Zenodo (respectively DOI: 10.5281/zenodo.10514225 and 10.5281/zenodo.10518169) and at www.teabagindex.org. The global map of initial decomposition rates (DOI: 10.5281/zenodo.10513802) and the stabilization factor (DOI: 10.5281/zenodo.10514018), are also published together with their meta data. All data are part of the Tea Bag Index community, that intends to collect TBI data and, therefore, is open to new contributions. The script used to perform the analyses reported here can be found as supplementary document.

ORCID

Judith M. Sarneel https://orcid.org/0000-0001-6187-499X

REFERENCES

Althuizen, I.H.J., Lee, H., Sarneel, J.M. & Vandvik, V. (2018) Long-term climate regime modulates the impact of short-term climate variability on decomposition in alpine grassland soils. *Ecosystems*, 21, 1580–1592.

Austin, A.T. & Vivanco, L. (2006) Plant litter decomposition in a semi-arid ecosystem controlled by photodegradation. *Nature*, 442, 555–558.

Bahram, M., Netherway, T., Hildebrand, F., Pritsch, K., Drenkhan, R., Loit, K. et al. (2020) Plant nutrient-acquisition strategies drive topsoil microbiome structure and function. *New Phytologist*, 227, 1189–1199.

Bardgett, R.D. & van der Putten, W.H. (2014) Belowground biodiversity and ecosystem functioning. *Nature*, 515, 505–511.

Berg, B., Berg, M.P., Bottner, P., Box, E., Breymeyer, A., Deanta, R.C. et al. (1993) Litter mass-loss rates in pine forests of Europe and Eastern United States—some relationships with climate and litter quality. *Biogeochemistry*, 20, 127–159.

Berg, B. & McClaugherty, C. (2020) *Plant litter, decomposition, humus formation, carbon sequestration*, 4th edition. New York, USA: Springer.

Buckeridge, K.M., Mason, K.E., McNamara, N.P., Ostle, N., Puissant, J., Goodall, T. et al. (2020) Environmental and microbial controls on microbial necromass recycling, an important precursor for soil carbon stabilization. *Communications Earth & Environment*, 1, 36.

Cebrian, J. (1999) Patterns in the fate of production in plant communities. *The American Naturalist*, 154, 449–468.

Cotrufo, M.F., Soong, J.L., Horton, A.J., Campbell, E.E., Haddix, M.L., Wall, D.H. et al. (2015) Formation of soil organic matter via biochemical and physical pathways of litter mass loss. *Nature Geoscience*, 8, 776–779.

Cotrufo, M.F., Wallenstein, M.D., Boot, C.M., Denef, K. & Paul, E. (2013) The Microbial Efficiency-Matrix Stabilization (MEMS) framework integrates plant litter decomposition with soil organic matter stabilization: do labile plant inputs form stable soil organic matter? *Global Change Biology*, 19, 988–995.

Daebeler, A., Petrová, E., Kinz, E., Grausenburger, S., Berthold, H., Sandén, T. et al. (2022) Pairing litter decomposition with microbial community structures using the Tea Bag Index (TBI). *The Soil*, 8, 163–176.

Djukic, I., Kepfer-Rojas, S., Schmidt, I.K., Larsen, K.S., Beier, C., Berg, B. et al. (2018) Early stage litter decomposition across biomes. *Science of the Total Environment*, 628-629, 1369–1394.

Duddigan, S., Alexander, P.D., Shaw, L.J., Sanden, T. & Collins, C.D. (2020) The Tea Bag Index-UK: using citizen/community science to investigate organic matter decomposition rates in domestic gardens. *Sustainability*, 12, 6895.

Duddigan, S., Shaw, L.J., Alexander, P.D. & Collins, C.D. (2020) Chemical underpinning of the tea bag index: an examination of the decomposition of tea leaves. *Applied and Environmental Soil Science*, 2020, 8.

Fanin, N., Bezaud, S., Sarneel, J.M., Cecchini, S., Nicolas, M. & Augusto, L. (2020) Relative importance of climate, soil and plant functional traits during the early decomposition stage of standardized litter. *Ecosystems*, 23, 1004–1018.

Foley, J.A. (2005) Integrated biosphere simulator model (IBIS), version 2.5. Available at: https://daac.ornl.gov/cgi-bin/dsviewer.pl?ds_id=8082020

Gessner, M.O., Chauvet, E. & Dobson, M. (1999) A perspective on leaf litter breakdown in streams. *Oikos*, 85, 377–384.

Gholz, H.L., Wedin, D.A., Smitherman, S.M., Harmon, M.E. & Parton, W.J. (2000) Long-term dynamics of pine and hardwood litter in contrasting environments: toward a global model of decomposition. *Global Change Biology*, 6, 751–765.

Gorelick, N., Hancher, M., Dixon, M., Ilyushchenko, S., Thau, D. & Moore, R. (2017) Google earth engine: planetary-scale geospatial analysis for everyone. *Remote Sensing of Environment*, 202, 18–27.

Harmon, M.E. (2016) LTER Intersite fine litter decomposition experiment (LIDET), 1990 to 2002 version 11. (ed. Site, AFL) Corvallis.

He, Y., Wang, X.H., Wang, K., Tang, S.C., Xu, H., Chen, A.P. et al. (2021) Data-driven estimates of global litter production imply slower vegetation carbon turnover. *Global Change Biology*, 27, 1678–1688.

Heimann, M. & Reichstein, M. (2008) Terrestrial ecosystem carbon dynamics and climate feedbacks. *Nature*, 451, 289–292.

Hobbie, S.E., Eddy, W.C., Buyarski, C.R., Adair, E.C., Ogdahl, M.L. & Weisenhorn, P. (2012) Response of decomposing litter and its microbial community to multiple forms of nitrogen enrichment. *Ecological Monographs*, 82, 389–405.

IPCC. (2022) Climate change 2022: impacts, adaptation, and vulnerability. In: Pörtner, H.-O., Roberts, D.C., Tignor, M., Poloczanska, E.S., Mintenbeck, K., Alegría, A., et al. (Eds.) *Contribution of working group II to the sixth assessment report of the intergovernmental panel on climate change, Cambridge, UK and New York, USA*, p. 3056.

Joly, F.X., Scherer-Lorenzen, M. & Hättenschwiler, S. (2023) Resolving the intricate role of climate in litter decomposition. *Nature Ecology & Evolution*, 7, 214–223.

Keuskamp, J.A., Dingemans, B.J.J., Lehtinen, T., Sarneel, J.M. & Hefting, M.M. (2013) Tea Bag Index: a novel approach to collect uniform decomposition data across ecosystems. *Methods in Ecology and Evolution*, 4, 1070–1075.

Kwon, T., Shibata, H., Kepfer-Rojas, S., Schmidt, I.K., Larsen, K.S., Beier, C. et al. (2021) Effects of climate and atmospheric nitrogen deposition on early to mid-term stage litter decomposition across biomes. *Frontiers in Forests and Global Change*, 4, 678480.

Le Noë, J., Manzoni, S., Abramoff, R., Bölscher, T., Bruni, E., Cardinael, R. et al. (2023) Soil organic carbon models need independent time-series validation for reliable prediction. *Communications Earth & Environment*, 4, 158.

Lenth, R.V., Bolker, B., Buerkner, P., Gine-Vasquez, I., Herve, M., Jung, M. et al. (2023) Emmeans: estimated marginal means, aka least-squares means.

Li, R.S., Guo, X.Y., Han, J.M., Yang, Q.P., Zhang, W.D., Yu, X. et al. (2023) Global pattern and drivers of stable residue size from decomposing leaf litter. *Catena*, 232, 107390.

Minasny, B., Malone, B.P., McBratney, A.B., Angers, D.A., Arrouays, D., Chambers, A. et al. (2017) Soil carbon 4 per mille. *Geoderma*, 292, 59–86.

Mori, T., Nakamura, R. & Aoyagi, R. (2022) Risk of misinterpreting the Tea Bag Index: field observations and a random simulation. *Ecological Research*, 37, 381–389.

Mueller, P., Schile-Beers, L.M., Mozdzer, T.J., Chmura, G.L., Dinter, T., Kuzyakov, Y. et al. (2018) Global-change effects on early-stage decomposition processes in tidal wetlands—implications from a global survey using standardized litter. *Biogeosciences*, 15, 3189–3202.

Njoroge, D.M., Chen, S.C., Zuo, J., Dossa, G.G.O. & Cornelissen, J.H.C. (2022) Soil fauna accelerate litter mixture decomposition globally, especially in dry environments. *Journal of Ecology*, 110, 659–672.

Ochoa-Hueso, R., Borer, E.T., Seabloom, E.W., Hobbie, S.E., Risch, A.C., Collins, S.L. et al. (2020) Microbial processing of plant remains is co-limited by multiple nutrients in global grasslands. *Global Change Biology*, 26, 4572–4582.

Olson, D.M., Dinerstein, E., Wikramanayake, E.D., Burgess, N.D., Powell, G.V.N., Underwood, E.C. et al. (2001) Terrestrial ecoregions of the worlds: a new map of life on Earth. *Bioscience*, 51, 933–938.

Parton, W., Silver, W.L., Burke, I.C., Grassens, L., Harmon, M.E., Currie, W.S. et al. (2007) Global-scale similarities in nitrogen release patterns during long-term decomposition. *Science*, 315, 361–364.

Parton, W.J., Hartman, M., Ojima, D. & Schimel, D. (1998) DAYCENT and its land surface submodel: description and testing. *Global and Planetary Change*, 19, 35–48.

Post, E., Alley, R.B., Christensen, T.R., Macias-Fauria, M., Forbes, B.C., Gooseff, M.N. et al. (2019) The polar regions in a 2 degrees C warmer world. *Science Advances*, 5, eaaw9883.

Prescott, C.E. (2010) Litter decomposition: what controls it and how can we alter it to sequester more carbon in forest soils? *Biogeochemistry*, 101, 133–149.

R Core Team. (2023) *R: a language and environment for statistical computing.* Vienna, Austria: R Foundation for Statistical Computing.

Robbins, C.J., Norman, B.C., Halvorson, H.M., Manning, D.W., Bastias, E., Biasi, C. et al. (2022) Nutrient and stoichiometric time series measurements of decomposing coarse detritus in freshwaters worldwide from literature published between 1976–2020 ver 1. (ed. Initiative, ED).

Sanchez, P.A., Ahamed, S., Carre, F., Hartemink, A.E., Hempel, J., Huising, J. et al. (2009) Digital soil map of the world. *Science*, 325, 680–681.

Sarneel, J.M., Barel, J.M., Duddigan, S., Keuskamp, J.A., Pastor Oliveras, A., Sanden, T. et al. (2023) Reasons to not correct for leaching in TBI; reply to Lind et al 2022. *Authorea*, 13, e10133.

Sarneel, J.M.J. & Veen, G.F.C. (2017) Legacy effects of altered flooding regimes on decomposition in a boreal floodplain. *Plant and Soil*, 421, 57–66.

Stockmann, U., Padarian, J., McBratney, A., Minasny, B., de Brogniez, D., Montanarella, L. et al. (2015) Global soil organic carbon assessment. *Global Food Security-Agriculture Policy Economics and Environment*, 6, 9–16.

Tang, H., Nolte, S., Jensen, K., Yang, Z., Wu, J. & Mueller, P. (2020) Grazing mediates soil microbial activity and litter decomposition in salt marshes. *Science of the Total Environment*, 720, 137559.

Thomas, H.J.D., Myers-Smith, I.H., Høye, T.T., Bon, M.P., Lembrechts, J., Walker, E.R. et al. (2023) Litter quality outweighs climate as a driver of decomposition across the tundra biome. *EcoEvoRxiv*.

Trofymow, J.A., Moore, T.R., Titus, B., Prescott, C., Morrison, I., Siltanen, M. et al. (2002) Rates of litter decomposition over 6 years in Canadian forests: influence of litter quality and climate. *Canadian Journal of Forest Research-Revue Canadienne De Recherche Forestiere*, 32, 789–804.

van den Brink, L., Canessa, R., Neidhardt, H., Knuver, T., Rios, R.S., Saldana, A. et al. (2023) No home-field advantage in litter decomposition from the desert to temperate forest. *Functional Ecology*, 37, 1315–1327.

van den Hoogen, J., Geisen, S., Routh, D., Ferris, H., Traunspurger, W., Wardle, D.A. et al. (2019) Soil nematode abundance and functional group composition at a global scale. *Nature*, 572, 194–198.

Veen, G.F., Freschet, G.T., Ordonez, A. & Wardle, D.A. (2015) Litter quality and environmental controls of home-field advantage effects on litter decomposition. *Oikos*, 124, 187–195.

SUPPORTING INFORMATION

Additional supporting information can be found online in the Supporting Information section at the end of this article.